Simulating Ca^+ ions in a Penning trap

Synne Sigstad Jørgensen & Rebecca Nguyen
(Dated: December 10, 2024)

The Penning trap is a device for confining charged particles with electric and magnetic fields. As we do not possess such a device, we study the trap by modeling it numerically. We simulate Ca^+ ion(s) trajectories using Runge-Kutta 4 and Forward Euler, where we found Runge-Kutta to correspond well to the analytical solution while Forward Euler deviates more. From the simulations, we create trajectory plots and phase space plots. The relative errors and error convergence rates are also investigated. We get an error convergence rate of 1.0006 and 1.4001 for Runge-Kutta 4 and Forward Euler respectively.

I. INTRODUCTION

In 1959, Hans G. Dehmelt built his first high vacuum magnetron trap and was soon able to trap electrons for about 10 seconds. He developed a simple description of the axial, magnetron and cyclotron motion of an electron in it. The inspiration came from F.M. Penning and the device was therefore named the Penning trap. This won Dehmelt a shared Nobel Prize in Physics in 1989 [1].

The Penning trap is a way of confining a charged particle, with the use of magnetic and electric fields. The instrument has been used as a tool for different experimental purposes, like measuring the magnetic moment of a proton to extremely high precision [2]. Newton's second law governs the motion of a particle confined in the Penning trap. This means that the time evolution of the particles can be solved using differential equations with complex solutions.

In this paper, we aim to understand how the trap operates and confines Ca^+ ions. We do not have access to such a device and will therefore study the particle motion using analytical and numerical methods, by solving the equations of motion for positively charged confined particles.

In section II we cover the physics background and present an algorithm that can be implemented in any programming language. Equations presented in this section are derived in section A. In section III we present results from our validation test and discuss our implemented algorithms. Finally, we summarize and discuss future work in section IV. All code developed for this paper can be found on our GitHub repository [1].

II. METHODS

The Penning Trap

We are working with confining a positive ion. Although a setup on the form shown in Figure 1 might seem intuitive, it can not be achieved. This is because it allows for negative divergence and hence negative density, as we have a relation $\nabla \cdot \vec{E} \propto \rho$ [3].

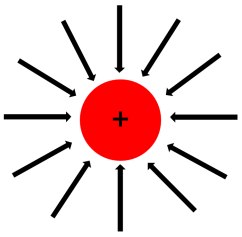

FIG. 1. This setup would not be possible to achieve in order to confine a positively charged particle, as it would allow for negative divergence of the electric field.

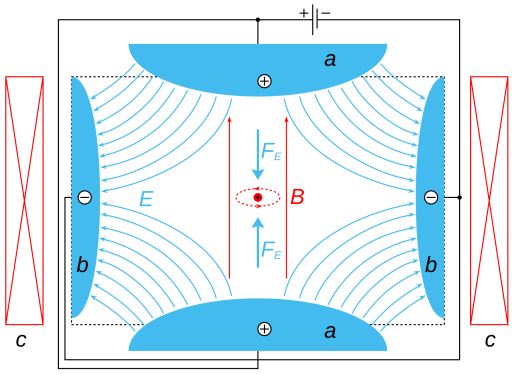

FIG. 2. The figure illustrates a Penning trap. The device trap uses both magnetic (red field lines) and electric (blue field lines) fields to confine the charged particle. Figure from [5].

Therefore, one must think alternatively, and this is where the Penning trap becomes useful. The Penning trap utilizes an electrostatic quadruple potential, and a homogeneous magnetic field to confine the charged particle [4]. An example setup can be seen in Figure 2.

In this setup, an electric field $\vec{E}$ confines the particle in the z-direction, and a magnetic field confines the particle in the xy-direction. The Lorentz force describes the total force

$$\mathbf{F} = q\mathbf{E} + q\mathbf{v} \times \mathbf{B} \tag{1}$$

where q represents the ion charge. We use a Penning trap

[1] https://github.uio.no/rebeccng/FYS4150/tree/main/project3

with an electric field described by an electric potential

$$V(x,y,z) = \frac{V_0}{2d^2}(2z^2 - x^2 - y^2) \tag{2}$$

where d describes the *characteristic dimension*. This is the length between the electrodes in the trap.

A. Equations of motion: Single particle

(*All equations in this section are derived in section A*).

The time evolution of a particle confined in the penning trap will be governed by Newton's second law, given by

$$m\ddot{\mathbf{r}} = \sum_i \mathbf{F}_i, \tag{3}$$

where m is the mass of the particle, $\ddot{\mathbf{r}}$ is the acceleration of the particle, and F_i denotes the forces the particle is subject to. We have a three-dimensional system, i.e. movement in x-y-and z direction The equations describing these motions are coupled, hence can we go from three equations of motion in 3D, given by

$$\begin{aligned} \ddot{x} &= \frac{1}{2}\omega_z^2 x + \omega_0 \dot{y} \\ \ddot{y} &= \frac{1}{2}\omega_z^2 y - \omega_0 \dot{x} \\ \ddot{z} &+ \omega_z^2 z = 0 \end{aligned} \tag{4}$$

to a complex function

$$\ddot{f} + i\omega_0 \dot{f} - \frac{1}{2}\omega_z^2 f = 0. \tag{5}$$

Here we have the expressions

$$\omega_0 \equiv \frac{qB_0}{m}, \quad \omega_z^2 \equiv \frac{2qV_0}{md^2} \tag{6}$$

for angular frequencies ω_0 and ω_z.

The general solution to Equation 5 is given by

$$f(t) = A_+ e^{-i(\omega_+ t + \phi_+)} + A_- e^{-i(\omega_- t + \phi_-)} \tag{7}$$

where ϕ_+, ϕ_- are constant phases, A_+, A_- are positive amplitudes and angular frequencies ω_+ and ω_- are given by

$$\omega_\pm = \frac{\omega_0 \pm \sqrt{\omega_0^2 - 2\omega_z^2}}{2}. \tag{8}$$

The physical coordinates are $x(t) = \mathrm{Re} f(t)$ and $y(t) = \mathrm{Im} f(t)$. It is necessary to obtain a bounded solution of the particle's movement in the xy-plane because $f(t)$ is diverging for $\omega_\pm \in \mathbb{C}$. We obtain the bounded solution by putting constraints on ω_0 and ω_z giving us

$$\frac{q}{m} > \frac{2V_0}{B_0 d^2}. \tag{9}$$

The upper and lower bounds of the particle's distance from the origin in the xy-plane are

$$R_+ = A_+ + A, \quad R_- = |A_+ - A_-|. \tag{10}$$

TABLE I. Comparison between global and local error of Forward Euler and Runge-Kutta 4.

Method	Local error	Global error
FE	$\mathcal{O}(h^2)$	$\mathcal{O}(h)$
RK4	$\mathcal{O}(h^5)$	$\mathcal{O}(h^4)$

B. Equations of motion: Multiple particles

In the case of a Penning trap with multiple particles, each particle will experience both the force from the external electric and magnetic field and the Coulomb force from all other particles. Thus, the equations of motion become

$$\begin{aligned} \ddot{x}_i - \omega_{0,i}\dot{y}_i - \frac{1}{2}\omega_{z,i}^2 x_i - k_e \frac{q_i}{m_i} \sum_{j \neq i} q_j \frac{x_i - x_j}{|\mathbf{r}_i - \mathbf{r}_j|^3} = 0, \\ \ddot{y}_i + \omega_{0,i}\dot{x}_i - \frac{1}{2}\omega_{z,i}^2 y_i - k_e \frac{q_i}{m_i} \sum_{j \neq i} q_j \frac{y_i - y_j}{|\mathbf{r}_i - \mathbf{r}_j|^3} = 0, \\ \ddot{z}_i + \omega_{z,i}^2 z_i - -k_e \frac{q_i}{m_i} \sum_{j \neq i} q_j \frac{z_i - z_j}{|\mathbf{r}_i - \mathbf{r}_j|^3} = 0, \end{aligned} \tag{11}$$

where i and j are particle indices. We solve this numerically by formulating the problem in terms of coupled, first-order differential equations

$$\begin{aligned} \dot{\mathbf{r}} &= \mathbf{v} \\ \dot{\mathbf{v}} &= \mathbf{F}/m. \end{aligned} \tag{12}$$

C. Algorithm

We use numerical methods to solve the coupled first-order differential equations shown in Equation 12. In particular, Runge-Kutta of the 4th order (RK4, Algorithm 1) and Forward Euler (FE, Algorithm 2). RK4 will be used to evolve our Penning Trap. We include Forward Euler for comparison when RK4 does not provide sensible results when developing the code. This allows us to check if the implementation of RK4 or some other part of the code is wrong.

Both methods are single-step methods meaning we only need the current step to further advance our system. The difference between the two is that FE requires one evaluation of f (here: the total force on a particle), whilst RK4 requires four. Though this gives a higher global error for RK4, it does provide a higher accuracy than FE allowing us to use a much larger step size in our computations. A weighted sum of the four evaluation points is used to compute the next time step. The form of the weighted combination comes from Simpson's rule for numerical integration.

Algorithm 1 Runge-Kutta 4th order for coupled equations

$x_0 \leftarrow [r_x, r_y, r_z]$ ▷ Initial position vector
$v_0 \leftarrow [v_x, v_y, v_z]$ ▷ Initial velocity vector
$h = t_{tot}/n$ ▷ Stepsize
for $i = 0, 1, 2, \ldots, n$ **do**
$k_{x,1} = hv_i$
$k_{v,1} = hf(t_i, x_i, v_i)$
$k_{x,2} = h(v_i + \frac{1}{2}k_{v,1})$
$k_{v,2} = hf(t_i + \frac{1}{2}h, x_i + \frac{1}{2}k_{x,1}, v_i + \frac{1}{2}k_{v,1})$
$k_{x,3} = h(v_i + \frac{1}{2}k_{v,2})$
$k_{v,3} = hf(t_i + \frac{1}{2}h, x_i + \frac{1}{2}k_{x,2}, v_i + \frac{1}{2}k_{v,2})$
$k_{x,4} = h(v_i + k_{v,3})$
$k_{v,4} = hf(t_i + h, x_i + k_{x,3}, v_i + k_{v,3})$
$x_{i+1} \leftarrow x_i + \frac{1}{6}(k_{x,1} + 2k_{x,2} + 2k_{x,3} + k_{x,4})$
$v_{i+1} \leftarrow v_i + \frac{1}{6}(k_{v,1} + 2k_{v,2} + 2k_{v,3} + k_{v,4})$

Algorithm 2 Forward Euler

$x_0 \leftarrow [r_x, r_y, r_z]$ ▷ Initial position vector
$v_0 \leftarrow [v_x, v_y, v_z]$ ▷ Initial velocity vector
$h = t_{tot}/n$ ▷ Step size
for $i = 0, 1, 2, \ldots, n$ **do**
$v_{i+1} \leftarrow v_i + hf_i$
$x_{i+1} \leftarrow x_i + hv_i$

Tools

We have utilized GitHub copilot to explain our code and help debug. We used the Python library `matplotlib` [6] to produce all illustrations in this report. In addition to using Grammarly to rewrite and check grammar.

III. RESULTS AND DISCUSSION

A. Specific analytic solution

To test our code, we consider a single particle with charge q and mass m which with the following initial conditions

$$\begin{aligned} \mathbf{r}_0 &= (x_0, y_0, z_0) = (x_0, 0, z_0) \\ \dot{\mathbf{r}} &= (\dot{x}_0, \dot{y}_0, \dot{z}_0) = (0, v_0, 0). \end{aligned} \tag{13}$$

From z_0 and $\dot{z_0}$ we obtain the specific solution of z

$$z(t) = z_0 \cos(\omega_z t) \tag{14}$$

The particle's movement in the xy-plane has the specific solution $f(t)$ given by

$$A_+ = \frac{v_0 + \omega_- x_0}{\omega_- - \omega_+}, \quad A_- = -\frac{v_0 + \omega_+ x_0}{\omega_- - \omega_+}, \tag{15}$$

$$\phi_+ = 0, \quad \phi_- = 0. \tag{16}$$

The numerical and analytical solution is comparable for a single particle in the Penning trap.

Parameter	Value
External magnetic field (B_0)	$9.65 \cdot 10^1 \frac{\mu}{(\mu s)e}$
Potential applied to the electrodes (V_0)	$2.41 \cdot 10^6 \frac{u(\mu m)^2}{(\mu s)^2 e}$
Characteristic dimension (d)	500 μm

TABLE II. Default parameters for our Penning trap set-up.

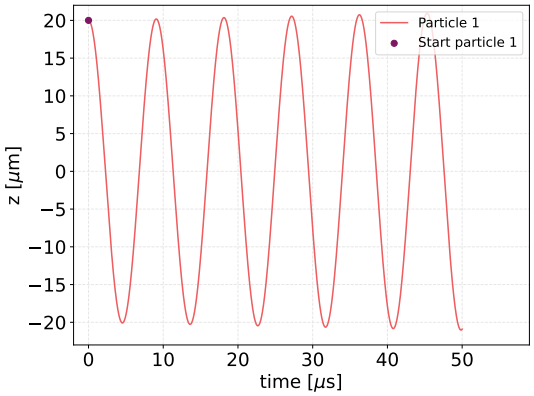

FIG. 3. The particle follows an oscillating motion in the z-direction as time passes. In the figure, the particle motion plotted is the one of the particle with initial position $\vec{r_1}$={20, 0, 20} and initial velocity $\vec{v_1}$={0, 25, 0}.

Our default Penning trap configuration can be seen in the Table II Given the parameters we obtain

$$\omega_z \approx 0.6935 \frac{1}{\mu s}. \tag{17}$$

B. One particle simulation

We start with the simplest case: a single Ca^+ ion in the Penning trap. In this case, only the external electric and magnetic fields will affect the particle. In Figure 3 we see that the particle follows an oscillating motion in the z-direction over the a time span of 50 μs, starting at the initial positions $\vec{r_1}$={20, 0, 20}μm and initial velocities $\vec{v_1}$={0, 25, 0}$\mu m/\mu s$. Since ω_z is expressed with only constants (Equation 6), the calculated value will also be constant. This constant value has been calculated in Equation 17. A constant ω_z in the expression given in Equation 14 would result in a cosinusoidal motion. Our results are therfore as expected, as a cosinusoidal pattern is verified through our simulation, and shown in Figure 3.

C. Two particle simulation

1. *Trajectory Plots*

For our next step, we simulate two Ca^+ ions in our Penning trap. We will first focus on the particle move-

ments in the $x-y$-plane. Our code gives us the possibility to choose whether to include particle interaction or not. Figure 4 illustrates the observed motion in the $x-y$-plane from our two particles in the Penning trap, when there is no particle interaction between the two. Based on Equation A17, we would expect orbital motion in the $x-y$-plane. The results shown in Figure 4 supports this theory, where we can see orbital motion for both Particle 1 and Particle 2, starting from their respective initial positions and velocities. The circular path followed counter clockwise is the magnetron motion (ω_-), and the smaller orbital motion each particle undergoes while following this counter clockwise trajectory is the cyclotron motion (ω_+) [7]. When we allow for particle interactions, we see in Figure 5 that the trajectories get distorted. This is because the two particles are now experiencing a repulsive Coulomb force due to both particles having a positive charge. The closer the particles are, the stronger the repulsive force be between them will be, as the force follows an inverse square law.

We have also plotted our results from the simulation using the RK4, in three dimensional plots. We consider both cases with and without particle interaction, and the results are shown in Figure 6 and Figure 7, respectively. Here the orbital motions in the $x-y$-plane and the oscillating motion in the z-plane is combined. At first glance, the motion of both particles look relatively messy and random. However, if we adjust the 3D-plots displaying the case without particle interaction so that it displays the $x-y$-plane with the z-direction "out" of the paper, we recognize a very similar pattern like the one in Figure 4. This adjustment has been done in Figure 8, to illustrate. The small differences is due to the adjustments being done by hand. We would obtain a similar result for the case with particle interaction as well.

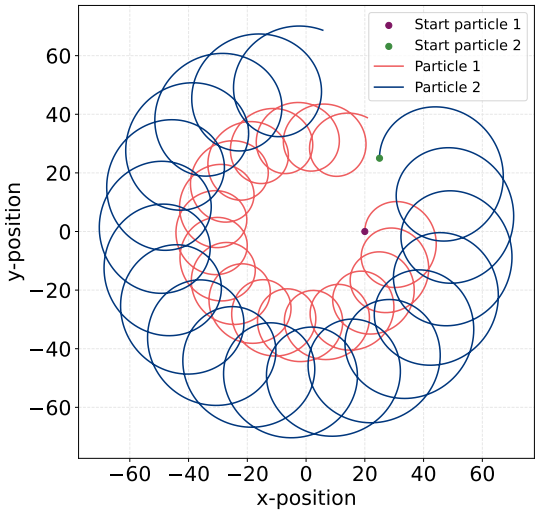

FIG. 4. Both particles in the trap follow orbital motions in the $x-y$-plane when there is no particle interaction. The resulting trajectory is due to magnetron and cyclotron motion.

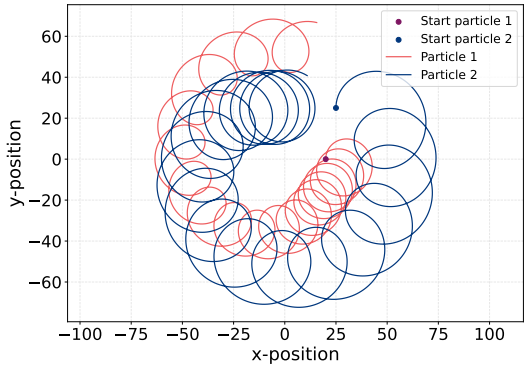

FIG. 5. The force between the particles are affecting each particle's motion. The orbital motions we saw with no particle interactions have now been distorted.

2. *Phase space plots*

We are also interested in how the particles behave in phase space, to get a better overview of the system. In Figure 9 and Figure 11 we see how the particles behave in respectively (x, v_x) and (z, v_z) phase space when there is no interaction between the particles. For the phase space plot in the z-direction, theory tells us that the velocity should be at a minimum when the particle is at its furthest from the center of the trap, and at a maximum the moment it passes the center. It is the same behaviour like we would expect in the simpler case of an object oscillating from a spring without damping or friction in classical mechanics. From Figure 9, we see that the particle in our Penning trap behaves as expected. Here it is shown for both Particle 1 and Particle 2 that when the particle is at the center the velocity peaks, and when it is at its furthest from the center, the velocity is at zero. The reason why it looks like the particle is moving further away from the center for each "round" the particle passes the center, is because of the overshoot resulting from our use of the RK4 method. Theoretically, as our initial position in e.g. the x-axis is 20μm, this should be the particle's maximum distance from the center throughout the simulation. But because of the overshoot, which can be seen slightly in Figure 3 and is properly shown in Figure 15, our calculations show that the particle moves further away from the center for each round. However, this is not what happens physically in the simulation; it is a consequence of using numerical methods. For the phase space plot in the z-direction when we allow for particle interaction, seen in Figure 10, we see that the neat orbits from Figure 9 have been distorted. This is because the Coulomb repulsive force affects the particles. In the plot where we allow for particle interaction, the maximum and minimum velocities and

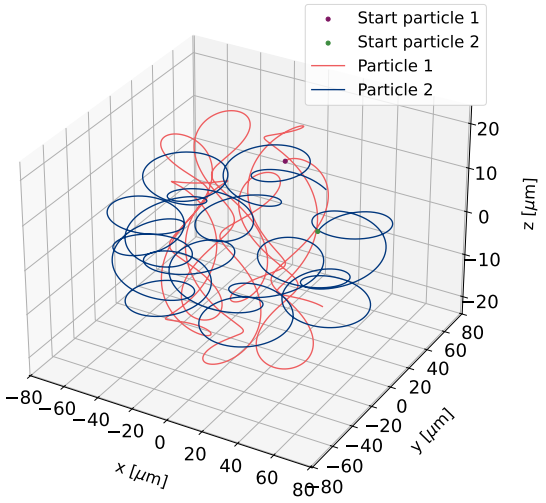

FIG. 6. The figure shows the motion of the two particles in three dimensions, without particle interaction.

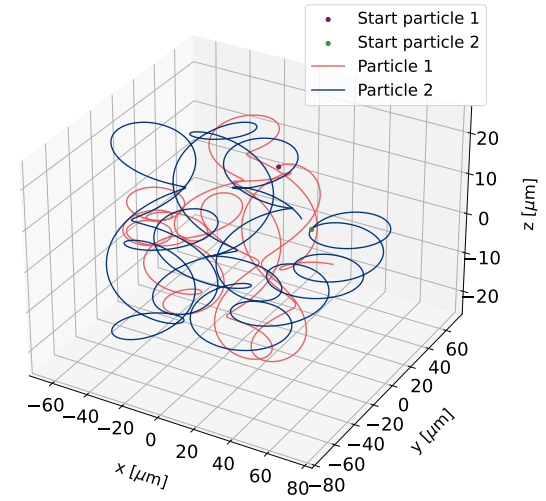

FIG. 7. The figure shows the motion of the two particles in three dimensions, with particle interaction

distances from the center has changed for both particles. In this case, both particles reach a maximum velocity above $15\mu\text{m}/\mu\text{m}$, although in the plot without interaction, e.g. Particle 2 only reaches a maximum absolute velocity of $5\mu\text{m}/\mu\text{s}$. This again leads to Particle to reaching a much larger maximum distance from the center,

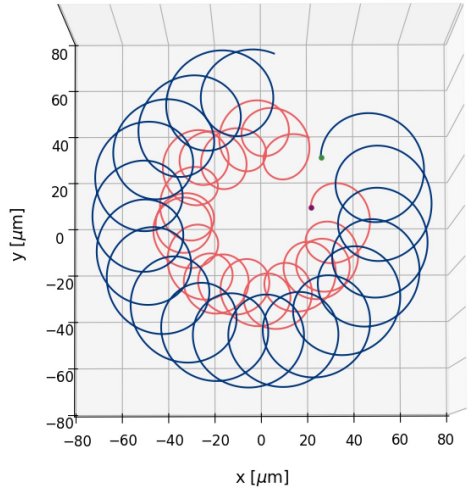

FIG. 8. The figure is to illustrate how the three dimensional plots can be adjusted to recognize the particle motion we deduced with the two dimensional plots.

now above 20μm in the positive direction, compared to about 8μm without particle interactions. The increase in distance from center and velocity is due to the Coulomb force, which accelerates the particle when it gets closer to the other particle, as the Coulomb force makes the particles repel each other. We can also see changes in both velocity and position for Particle 1 due to this force when comparing the two plots. For the phase space in the x-direction, both the magnetron and cyclotron motion contributes to the variation in velocity. The case without particle motion is shown in Figure 11, and the case with particle interaction is shown in Figure 12. For the latter, we see some of the same tendencies as for the phase space plots: e.g can we see that Particle 1 reaches a higher maximum velocity when affected by the Coulomb force, as well as a larger absolute distance away from the center, due to acceleration from the force.

D. Comparing numerical and analytical methods

Based on our theory, we would expect the RK4 method to be a more precise method than the FE method over time, as explained in section II C. To check if our hypothesis is correct, we have in Figure 15 plotted a comparison between the analytical results, the FE method results and the RK4 method results. Here, the simulations and calculations have been carried out with steps n_k of n_1=4000, n_2=8000, n_3=16000 and n_4=32000. From this plot we can deduce multiple facts. Firstly, the plots indicate that the various methods have been implemented correctly, as they all give the same results (to the degree we would expect, as the numerical methods are likely to overshoot). Secondly, it indicates that the errors are smaller for smaller step sizes. We see that both the RK results and the FE results are closer to the analytical re-

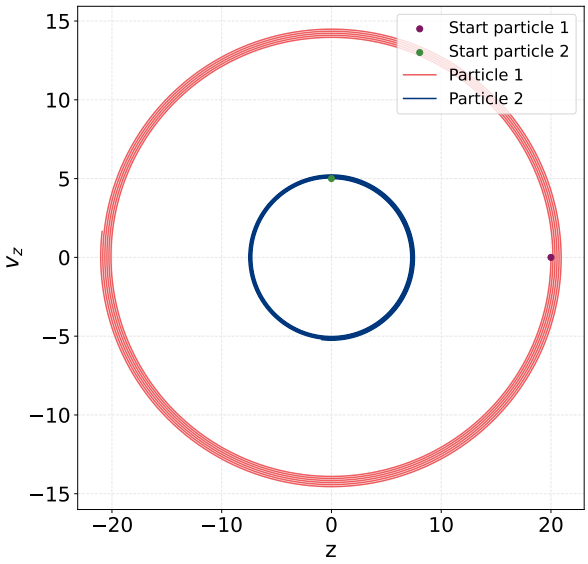

FIG. 9. The figure displays the behavior of Particle 1 and Particle 2 in phase space (z, v_z) when there are no interactions between the particles.

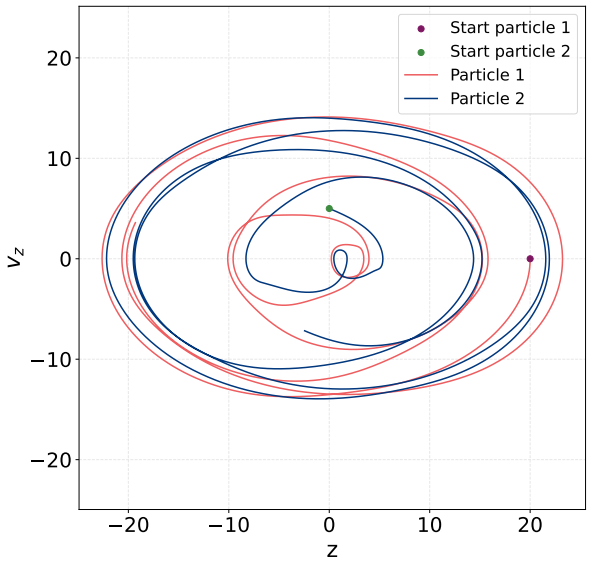

FIG. 10. The figure illustrates how the force between the particles are affecting each particle's motion. The orbital motions we saw with no particle interactions have now been distorted.

sults for the plot where the number of steps is 32000 compared to the plot where the number of steps is 4000. Because the time is the same (50μs), this means the step size decreases when we increase the number of steps. Thirdly, we see that the errors increase over time, both for the RK and the FE method. And as expected, the error for the FE methos increases more than the RK method over time.

E. Relative error and error convergence rate

The relative error ϵ_{rel} is calculated using

$$\epsilon_{rel}=\frac{|r_a - r_n|}{r_a}, \tag{18}$$

where r_a is the particle distance from the center r calculated with analytical data and r_n is r calculated with numerical data, i.e. data obtained with the Forward Euler or Runge-Kutta 4 method. The distance r is obtained from

$$r=\sqrt{x^2+y^2+z^2}, \tag{19}$$

where x, y, and z is the particle positions obtained through the simulation. The relative error in r_i is plotted in Figure 13 and Figure 14, for the Runge-Kutta method and Forward Euler method respectively. The variation is expected, considering the oscillating z-motion and orbital x-motion calculated discussed earlier. As the particle moves closer to the center of the trap, i.e. when r gets close to zero, the divisor in Equation 18 gets closer to zero, and hence will the relative error be large at these points. Hence are the spikes observed in the graphs for the relative errors expected. The relative errors obtained in our simulation also agree with our background knowledge, from which we would expect that the Forward Euler method would yield larger relative errors than the Runge-Kutta 4 method. In fact, from our results, the relative errors in the FE method are massive; between 40 and 50 μs it even surpasses a relative error of 100%, when the number of steps is 4000. However, as the same data for the Forward Euler method is used for the comparison in Figure 15 and the relative errors in Figure 14, we should expect this to be a correct graph for the relative error, assuming we have done the error calculations correctly. In comparison, the largest relative error for the RK4 method was a bit over 4%.

The error convergence rate describes how fast the difference between the analytical solution and our numerically calculated solutions goes to zero [8]. It is given by

$$r_{err} = \frac{1}{3}\sum_{k=2}^{4}\frac{\log(\Delta_{\max,k}/\Delta_{\max,k-1})}{\log(h_k/h_{k-1})}, \tag{20}$$

where h_k represent the step size for number of steps n_k and

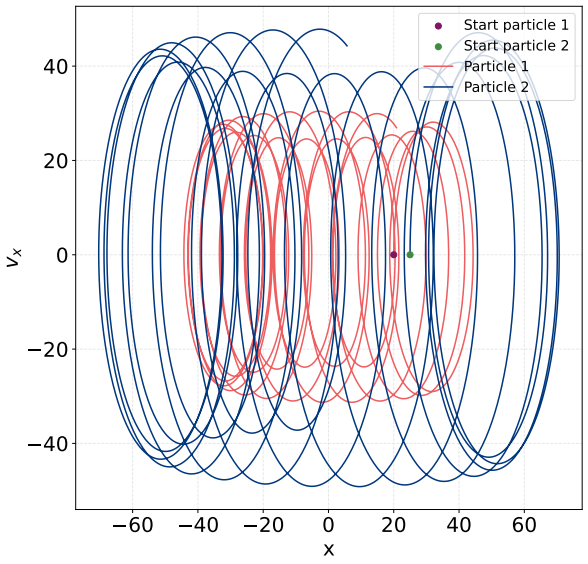

FIG. 11. The figure displays the behavior of Particle 1 and Particle 2 in phase space $(x,\, v_x)$ when there are no interactions between the particles.

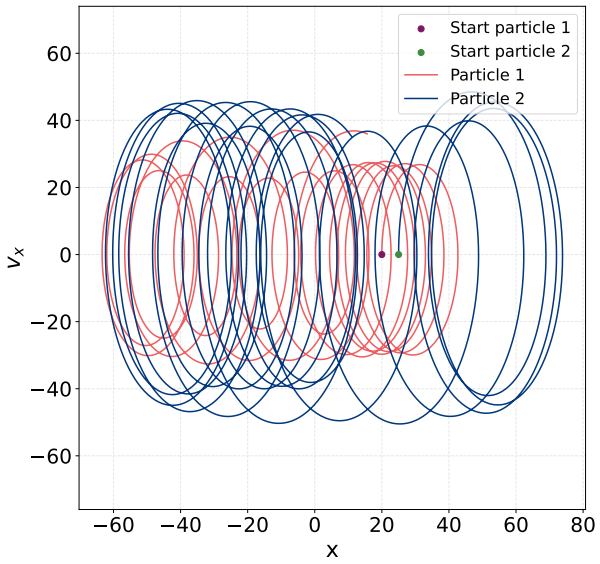

FIG. 12. The figure displays Particle 1 and Particle 2 behaviour in phase space $(x,\, v_x)$ when there are interactions between the particles.

$$\Delta_{\max,k} \;=\; \max\,|\mathbf{r}_{i,\text{exact}} - \mathbf{r}_i| \tag{21}$$

is the maximum error of the simulation with step size h_k, when taken over all time steps i. A higher value for the convergence rate would be desired, as this would mean that the difference between the analytical and numerical solution would go towards zero faster as the step size decreases. However, our results for the convergence rate is 1.0006 and 1.4001 for the Runge-Kutta 4 method and the Forward Euler method respectively. This means that the error in the FE method seems to be converging faster than the error in the RK4. This seems counter-intuitive, as our background knowledge tells us that the RK4 method should be more precise as the step size is decreasing. Hence would we expect a larger value for the error convergence rate for the RK4 method than for the FE method. Therefore, our results can indicate that something has gone wrong in our calculations of the errors or the error convergence rate.

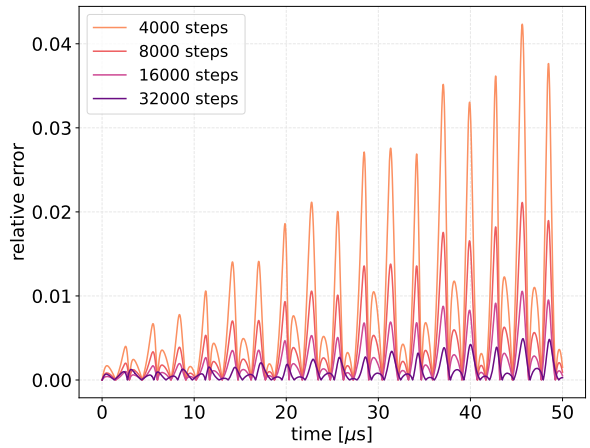

FIG. 13. Relative error in r for each time step, when the Runge-Kutta 4 method is used as the numerical method. The relative error is given for four given numbers of time steps in the simulations.

IV. CONCLUSION

We have in this paper simulated a Penning trap containing one or two identical Ca^+ ions. The simulations have been carried out using mainly the Runge-Kutta 4 numerical method, with number of steps being 4000, 8000, 16000 or 32000. The Penning trap is set up so that we have been able to choose whether to include interaction between the particles or not. When not including particle interaction, our results have shown orbital motions in the $x-y$-direction, and oscillating motion in the z-direction. This behavior agrees with the theoretical background we have presented. When including particle interaction, we have seen in our results that the Coulomb force between the both positively charged particles makes them repel each other, and the trajectories are distorted. We have also investigated the particles in phase space. When particle interactions are included, our results show

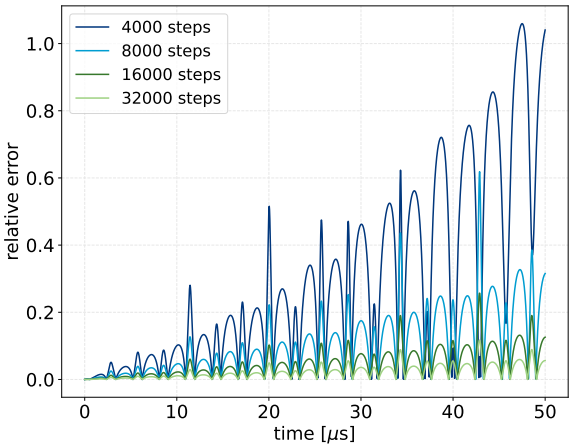

FIG. 14. Relative error in r for each time step, when the Forward Euler method is used as the numerical method. The relative error is given for four given numbers of time steps in the simulations.

how the particles may accelerate or change trajectories due to the Coulomb force. We have also seen how the velocities of the particles are related to their distance from the center.

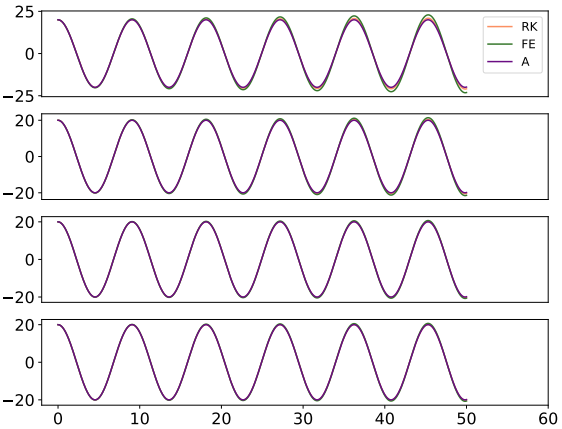

FIG. 15. Comparison of the Runge Kutta 4 method, the Forward Euler method and the analytical method. Starting from the top, the plots show the results for when number of steps n_k is n_1=4000, n_2=8000, n_3=16000, n_4=32000 respectively. Here, "RK" represents Runge-Kutta 4, "FE" represents Forward Euler and "A" represents analytical solution.

We have compared the results from the Runge-Kutta 4 method to a derived analytical method and the Forward Euler numerical method, where our results show that the relative errors for the FE method are larger than for the RK4 method. Overall, the errors for the RK4 method were shown to be quite small, while the errors for the FE method were very large. The resulting error convergence rates from these error calculations were 1.0006 and 1.4001 for Runge-Kutta 4 and Forward Euler respectively. This result is not consistent with the rest of our error calculations and background theory, as we predict RK4 to be the more precise method, and hence have a larger convergence error rate.

Further testing of our Penning trap beyond the basics presented in this paper remains a topic for future work. In particular, by subjecting the system to a time-dependent electromagnetic field. The interest is to study the occurrence of resonance phenomena and loss of trapped particles. Additionally, we would like to see to see how Coulomb interaction impacts these effects.

[1] Hans g. dehmelt biographical. https://www.nobelprize.org/prizes/physics/1989/dehmelt/biographical/. Accessed on October 22, 2024.
[2] Georg Schneider, Andreas Mooser, Matthew Bohman, Natalie Schön, James Harrington, Takashi Higuchi, Hiroki Nagahama,

Stefan Sellner, Christian Smorra, Klaus Blaum, Yasuyuki Matsuda, Wolfgang Quint, Jochen Walz, and Stefan Ulmer. Double-trap measurement of the proton magnetic moment at 0.3 parts per billion precision. *Science*, 2017.

[3] A Kvellestad. Lecture Notes FYS3150 - Computational Physics, Fall 2024.

[4] Lowell S. Brown and Gerald Gabrielse. Geonium theory: Physics of a single electron or ion in a penning trap. *Rev. Mod. Phys.*, 1986.

[5] Arian Kriesch. Penning trap, 2024. File: **PenningTrap.svg**.

[6] J. D. Hunter. Matplotlib: A 2d graphics environment. *Computing in Science & Engineering*, 9(3):90–95, 2007.

[7] V Yu Kozlov. WITCH, a Penning trap for weak interaction studies, 2005. Presented on 21 Nov 2005.

[8] Jasbir S. Arora. 8 - numerical methods for unconstrained optimum design. In *Introduction to Optimum Design (Second Edition)*, pages 277–304. Academic Press, San Diego, second edition edition, 2004.

Appendix A: The equations of motion for a single particle

The force from an electric field $\mathbf{E}$ and magnetic field $\mathbf{B}$ acting on a particle with charge q is described by the Lorentz force

$$F = q\mathbf{E} + q\mathbf{v} \times \mathbf{B}. \tag{A1}$$

The differential equations governing the time evolution of the particle's position, i.e. equations of motion, are derived from Newton's second law of motion and Lorentz force

$$m\ddot{\mathbf{r}} = q\mathbf{E} + q\mathbf{v} \times \mathbf{B}, \tag{A2}$$

where $\mathbf{v}$ denote the particle velocity. A homogeneous magnetic field is imposed in the z-direction, $\mathbf{B} = B_0\hat{e}_z$. The electric field is related to the electric potential through the following relation

$$\begin{aligned}\mathbf{E} &= -\nabla V = -\nabla \frac{V_0}{2d^2}(2z^2 - x^2 - y^2) \\ &= -\frac{\cancel{4}^{2}V_0 z}{\cancel{2}d^{\cancel{2}}}\hat{e}_z + \frac{\cancel{2}V_0}{\cancel{2}d^{\cancel{2}}}x\hat{e}_x + \frac{\cancel{2}V_0}{\cancel{2}d^{\cancel{2}}}y\hat{e}_y \\ &= \frac{V_0}{d^2}(x\hat{e}_x + y\hat{e}_y - 2z\hat{e}_z),\end{aligned} \tag{A3}$$

where ∇ denotes the gradient operator. The second term in the Lorentz force can be written as

$$\begin{aligned}q\mathbf{v} \times \mathbf{B} &= q\mathbf{v} \times B_0\hat{e}_z \\ &= q((\dot{x}\hat{e}_x + \dot{y}\hat{e}_y + \dot{z}\hat{e}_z) \times B_0\hat{e}_z) \\ &= qB_0(\dot{y}\hat{e}_x - \dot{x}\hat{e}_y).\end{aligned} \tag{A4}$$

By combining Equation A3 and Equation A4 we obtain an expression for EoM

$$m\ddot{\mathbf{r}} = q\left(\frac{V_0}{d^2}(x\hat{e}_x + y\hat{e}_y - 2z\hat{e}_z)\right) + qB_0(\dot{y}\hat{e}_x - \dot{x}\hat{e}_y), \tag{A5}$$

which give separate equations for $\ddot{x}$, $\ddot{y}$ and $\ddot{z}$ as seen in Equation A7, Equation A8 and Equation A6 below:

$$\begin{aligned}\ddot{z} &= -\frac{qV_0 2z}{md^2} \\ 0 &= \ddot{z} + \omega_z^2 z\end{aligned} \tag{A6}$$

$$\begin{aligned}m\ddot{x} &= \frac{qV_0 x}{d^2} + q\dot{y}B_0 \quad | \cdot \frac{1}{m} \\ \ddot{x} &= \frac{qV_0}{md^2}x + \frac{qB_0}{m}\dot{y} \\ \ddot{x} &= \frac{1}{2}\omega_z^2 x + \omega_0\dot{y} \\ \ddot{x} &= \frac{1}{2}\omega_z^2 x + \omega_0\dot{y}\end{aligned} \tag{A7}$$

$$\begin{aligned}m\ddot{y} &= \frac{qV_0 y}{d^2} - q\dot{x}B_0 \quad | \cdot \frac{1}{m} \\ \ddot{y} &= \frac{qV_0}{md^2}y - \frac{qB_0}{m}\dot{x} \\ \ddot{y} &= \frac{1}{2}\omega_z^2 y - \omega_0\dot{x} \\ \ddot{y} &= \frac{1}{2}\omega_z^2 y - \omega_0\dot{x}\end{aligned} \tag{A8}$$

Equation A6 is a second-order differential equation for a simple harmonic oscillator with a general solution given by

$$z(t) = A\sin(\omega_z t) + B\cos(\omega_z t), \tag{A9}$$

where the initial conditions determine A and B.

$$\omega_0 \equiv \frac{qB_0}{m}, \quad \omega_z^2 \equiv \frac{2qV_0}{md^2} \tag{A10}$$

Introducing $f = x + iy$ allows us to combine Equation A7 and Equation A8 into a single differential

$$\begin{aligned} \ddot{f} &= \ddot{x} + i\ddot{y} \\ &= \underbrace{\omega\dot{y} + \frac{1}{2}w_z^2 y}_{Equation\ A7} + i\left(\underbrace{-\omega_o\dot{x} + \frac{1}{2}w_z^2 y}_{Equation\ A8}\right) \\ &= \omega_o(\underbrace{\dot{y} - i\dot{x}}_{=-i\dot{f}}) + \frac{1}{2}w_z^2(\underbrace{x + iy}_{=f}) \\ \ddot{f} + i\omega_0\dot{f} - \frac{1}{2}\omega_z^2 f &= 0. \end{aligned} \tag{A11}$$

The general solution to Equation A11 is given by

$$f(t) = A_+ e^{-i(w_+ t + \phi_+)} + A_- e^{-i(w_- t + \phi_-)}, \tag{A12}$$

where ϕ_+ and ϕ_- are constant phases. The amplitudes A_+ and A_- are positive and,

$$\omega_\pm = \frac{\omega_0 \pm \sqrt{\omega_0^2 - 2\omega_z^2}}{2}. \tag{A13}$$

The physical coordinates of the particle are

$$x(t) = \mathrm{Re}f(t) + \mathrm{Im}f(t) \tag{A14}$$

It is necessary to find a bounded solution for ω_0 and ω_z in the xy-plane, i.e. where $|f(t)| < \infty$ as $t \to \infty$. For complex values of $\omega_\pm$ the solution diverges. Thus, we require $\omega_\pm \in \mathbb{R}$ and this is fulfilled when $\omega_0^2 - 2\omega_z^2 > 0$,

$$\omega_0^2 - 2\omega_z^2 > 0 \Rightarrow \omega_0 > 2\omega_z^2 \tag{A15}$$

$$\begin{aligned} \left(\frac{qB_0}{m}\right)^2 &> \frac{2qV_0}{md^2} \\ \frac{q}{m} &> \frac{2V_0}{B_0 d^2}. \end{aligned} \tag{A16}$$

Given Equation A14, we can find upper R_+ and lower R_- bounds of the particle's distance origin. Using Euler's formula, we begin by writing out $f(t)$ to find expressions for $x(t)$ and $y(t)$. For simplicity, we define $\alpha = \omega_+ t + \phi_+$ and $\beta = \omega_- t + \phi_-$.

$$\begin{aligned} f(t) &= A_+(\cos\alpha - i\sin\alpha) + A_-(\cos\beta - i\sin\beta) \\ &= \underbrace{A_+\cos\alpha + A_-\cos\beta}_{\mathrm{Re}f(t)\Rightarrow x(t)} - i\underbrace{(A_+\sin\alpha + A_-\sin\beta))}_{\mathrm{Im}f(t)\Rightarrow y(t)} \end{aligned} \tag{A17}$$

Distance from origin R is the following

$$\begin{aligned} R^2 &= x^2 + y^2 \\ &= A_+^2\cos^2\alpha + 2A_+A_-\cos\alpha\cos\beta + A_-^2\cos^2\beta + A_+^2\sin^2\alpha + 2A_+^2\sin\alpha\sin\beta + A_-^2\sin\beta \\ &= A_+^2(\underbrace{\cos^2\alpha + \sin^2\alpha}_{=1}) + 2A_+A_-(\underbrace{\cos\alpha\cos\beta + \sin\alpha\sin\beta}_{=\cos(\alpha-\beta)}) + A_-^2(\underbrace{\cos^2\beta + \sin^2\beta}_{=1}) \\ &= A_+^2 + A_-^2 + 2A_+A_-\cos(\alpha - \beta). \end{aligned} \tag{A18}$$

The R_+ and R_- occur when $\cos(\alpha - \beta)$ reach its maximum and minimum,

$$R = \begin{cases} R_+, & \alpha - \beta = 0 \\ R_-, & \alpha - \beta = \pi. \end{cases} \tag{A19}$$

Thus, the upper and lower bound of the particle's distance from the origin is

$$\begin{aligned} R_+ &= \sqrt{(A_+ + A_-)^2} = A_+ + A_- \\ R_- &= \sqrt{(A_+ - A_-)^2} = |A_+ - A_-|. \end{aligned} \tag{A20}$$